



HAL
open science

Precipitation-hardness map for Al–Cu–Mg alloy (AA2024-T3)

Vladimir A. Esin, L. Briez, Mohamed Sennour, Alain Köster, E. Gratiot,
Jérôme Crépin

► **To cite this version:**

Vladimir A. Esin, L. Briez, Mohamed Sennour, Alain Köster, E. Gratiot, et al.. Precipitation-hardness map for Al–Cu–Mg alloy (AA2024-T3). *Journal of Alloys and Compounds*, 2021, 854, pp.157164. 10.1016/j.jallcom.2020.157164 . hal-03084115

HAL Id: hal-03084115

<https://minesparis-psl.hal.science/hal-03084115>

Submitted on 17 Oct 2022

HAL is a multi-disciplinary open access archive for the deposit and dissemination of scientific research documents, whether they are published or not. The documents may come from teaching and research institutions in France or abroad, or from public or private research centers.

L'archive ouverte pluridisciplinaire **HAL**, est destinée au dépôt et à la diffusion de documents scientifiques de niveau recherche, publiés ou non, émanant des établissements d'enseignement et de recherche français ou étrangers, des laboratoires publics ou privés.



Distributed under a Creative Commons Attribution - NonCommercial 4.0 International License

Precipitation-hardness map for Al-Cu-Mg alloy (AA2024-T3)

V.A. Esin^{a,*}, L. Briez^{a,b}, M. Sennour^a, A. Köster^a, E. Gratiot^b, J. Crépin^a

^a*MINES ParisTech, PSL University, Centre des Matériaux (CNRS UMR 7633), Évry, France*

^b*Dassault Aviation, Saint-Cloud, France*

Abstract

By combining differential scanning calorimetry analysis and high-resolution transmission electron microscopy observations, the precipitation map for Al-Cu-Mg alloy (AA2024-T3) is obtained for a wide temperature range from 85 to 250 °C and ageing durations from 1 to 10000 hours. For the first time, the appearance of equilibrium S-Al₂CuMg phase is observed at 85 °C from 1000 hours of ageing. Hardness values superposed with the precipitation map reveal that the maximum hardness for all studied temperatures is located at the frontier between S-phase + Guinier-Preston-Bagaryatski (GPB) zones and S-phase regions.

Keywords:

2024 aluminium alloy, precipitation, co-clusters, GPB zones, hardness

1. Introduction

Wrought aluminium alloys are widely used in aeronautics and automotive industry due to their low cost and low density to strength ratio. In recent years, more and more parts usually made of other materials were replaced or are in the process of being replaced by parts made of aluminium alloys to decrease weight and, as a result, fuel consumption. In this scope, there is a number of attempts to increase service temperatures of the aluminium alloys often limited to 200 °C. This is achieved mostly through the optimisation of alloy compositions and/or the development of new heat treatments. Such optimisation is often based on the established knowledge of the industrially used alloys, namely, their advantages and limitations [1, 2].

The commercial 2024 aluminium alloy (AA2024) is one of the most used alloys in aircraft manufacturing for fuselage applications. The range of service temperature is usually considered to

*Corresponding author

Email address: vladimir.esin@mines-paristech.fr (V.A. Esin)

12 be between -55 and 85 °C for service lifetimes up to 20000 hours. AA2024 inherits its mechanical
 13 properties from the precipitation of hardening S-Al₂CuMg phase obtained through an appropriate
 14 heat treatment. Usually, such a heat treatment includes homogenisation around 500 °C followed by
 15 quenching and ageing at different temperatures ranging from room temperature to 200 °C. During
 16 ageing, hardening occurs and its kinetics depends strongly on temperature and time.

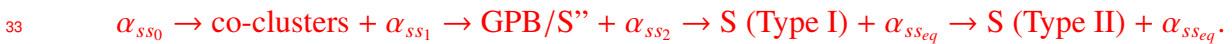
17 A number of different studies have been published so far on the ageing behavior of AA2024.
 18 Particular attention was paid to the precipitation sequence and the evolution of mechanical prop-
 19 erties as a function of ageing conditions [3–9]. It is well known that the formation of stable S-
 20 Al₂CuMg phase is preceded by the appearance of Cu-Mg co-clusters, Guinier-Preston-Bagaryatski
 21 (GPB) zones as well as different metastable S-phase precursors like S' and S'' [10]. **The original**
 22 **precipitation sequence for this type of alloys, first proposed by Bagaryatsky, was as follows [10]:**



24 where α_{ss} corresponds to supersaturated aluminum based solid solution. However, no study could
 25 reliably reveal the existence of S'' phase. Moreover, the difference between metastable S' and
 26 stable S phases relied on slight variations in lattice parameters. Therefore, another precipitation
 27 sequence was proposed taking into account these experimental uncertainties [10, 11]:



29 Recently, two types of stable S phase were reported to be able to form as a function of Si content
 30 and work hardening [7, 12–14]. Therefore, the exact precipitation sequence depends on alloy com-
 31 position and ageing conditions and is still under debate for AA2xxx-type alloys. **It is commonly**
 32 **written, according to the expression below [10–12, 14, 15]**



34 Despite the relatively low service temperature range (between -55 and 85 °C), **most of the stud-**
 35 **ies on ageing in AA2024 alloys focused on one or two ageing conditions in a narrow temperature**

36 range (often limited to temperatures between 120 and 200 °C) and to durations rarely exceeding
37 1000 hours. Moreover, a comparison of a number of results available in the literature for differ-
38 ent ageing conditions is difficult due to differences in composition (even minor) of AA2024 used
39 in different studies that can affect the kinetics of phase transformations. It seems however that
40 a detailed understanding of different evolutions occurring during ageing in the alloy of the *same*
41 composition at temperatures and durations close to service ones is essential for better controlling
42 of the service lifetime.

43 Therefore, the aim of the present work is to study phase transformations and the associated evo-
44 lution of mechanical properties in an AA2024 alloy for the temperature range and ageing durations
45 covering all possible service conditions (including unintended heating to very high temperatures)
46 ranging from 85 (upper service limit) to 250 °C for durations varying from 1 to 10000 hours for
47 each temperature. The obtained results will be presented in the form of a precipitation-hardness
48 map as a function of time and temperature.

49 **2. Material and methods**

50 The AA2024 alloy (Al-4.4Cu-1.4Mg-0.51Mn-0.12Fe-0.11Zn-0.07Si-0.04Ti wt. %) was sup-
51 plied in sheets of 2.5 mm in thickness. The alloy was homogenised at 495 °C during 30 min,
52 water quenched, strained approximately 3 % and aged at room temperature to obtain the standard
53 T3 state. It is worth noting that the sheets had been stored at room temperature for several years
54 after T3 heat treatment and before being used in this study. Therefore, the natural ageing can be
55 supposed completely finished.

56 The alloy composition as well as the aluminium matrix composition before thermal ageing
57 were obtained using Electron Probe Microanalyzer CAMECA SX100 operated at 15 kV with
58 probe current of 40 nA.

59 The ageing treatment was carried out in atmospheric air and the temperature was controlled
60 by a K-type thermocouple (the variations did not exceed 5 °C). The hardness was measured using

61 Wolpert DIA TESTOR 2 RC tester equipped with a tungsten carbide spheric indenter of 1 mm in
62 diameter. A force of 15 N was applied during 15 s and at least 5 measurements were taken. The
63 phase transformations occurring during ageing were studied using Differential Scanning Calorime-
64 try (DSC) [16] (Netzsch 224223 Jupiter). Samples of AA2024 weighing 20 mg were heated at a
65 constant rate of $10\text{ }^{\circ}\text{C min}^{-1}$ under Ar from room temperature to $450\text{ }^{\circ}\text{C}$. The baseline was obtained
66 using Al_2O_3 powder.

67 To verify the conclusions made using DSC experiments, High-Resolution Transmission Elec-
68 tron Microscopy (HRTEM) observations were carried out using FEI TECNAI F20-ST apparatus
69 operated at 200 kV. The foils for the observations were initially mechanically thinned to a thick-
70 ness of $120\text{ }\mu\text{m}$ and electrochemically jet polished in a mixture of nitric acid and methanol (1:3)
71 at $-30\text{ }^{\circ}\text{C}$ using a voltage of 9 mV.

72 **3. Results and discussion**

73

74 *3.1. Phases expected at equilibrium*

75 At equilibrium, the nature of the precipitates in ternary Al-Cu-Mg alloys might be predicted
76 from Cu/Mg ratio (using weight content of elements) [10]:

- 77 • for the alloys where $1.5 < \text{Cu/Mg} < 4$, only S- Al_2CuMg phase should be observed;
- 78 • if $4 < \text{Cu/Mg} < 8$, S- Al_2CuMg phase together with θ - Al_2Cu should form;
- 79 • for the alloys with the ratio $\text{Cu/Mg} > 8$, T- Al_6CuMg_4 and β - $\text{Al}_{12}\text{Mg}_{17}$ phases should appear
80 leading to a dramatic decrease of mechanical properties.

81 For the studied AA2024 alloy, $\text{Cu/Mg}=3.1$ and, thus, only S- Al_2CuMg should be expected at
82 equilibrium.

83 On the other hand, thermodynamic calculations can be used as well to predict phase equilibria
84 for different ageing temperatures. Such calculations were carried out using Thermo-Calc software
85 coupled with TCAL4 database. The concentrations of major alloying elements (Cu, Mg, Mn) in
86 the aluminium matrix¹ as-measured by Electron Probe Microanalyser in initial T3 state were used
87 as input so as to only consider solute that is available for the formation of new precipitates. The
88 calculated volume fraction of phases (with the exception of FCC aluminium solid solution) as a
89 function of temperature in the temperature range of interest is shown in Fig. 1. The calculations
90 show that S-Al₂CuMg, θ -Al₂Cu, Al₁₂Mn phases can be formed. Moreover, it can be observed that
91 the change in volume fractions of these phases is not significant between 85 and 250 °C (compare,
92 for example, 5 and 5.8 % of S at 85 and 250 °C, respectively). It is then possible to assume that the
93 equilibrium state should be the same for all the studied conditions in terms of nature of phases and
94 their fractions. It is worth noting that, contrary to the data reported in Fig. 1, the θ -Al₂Cu was not
95 observed for any ageing condition during experimental study presented below in agreement with
96 predictions using Cu/Mg ratio from Ref. [10] as described above. It might be associated to its low
97 fraction (< 1 % vol., according to Fig. 1) which makes it difficult to detect this phase surrounded
98 by the precipitates of other phases. Al₁₂Mn phase corresponds to so-called fine dispersoids which
99 are formed during the alloy processing. They are used to control the grain size by resisting to grain
100 boundary migration [10, 17, 18]. Therefore, the dispersoids were already present in the aluminium
101 matrix in initial T3 state and were not evolving during ageing in the temperature range used for
102 the experimental study.

103

104 3.2. Precipitation state after ageing

105 An example of recorded heat flux as a function of temperature during DSC experiment for
106 AA2024 in initial T3 state is shown in Fig. 2. It agrees well with the DSC curves reported in

¹Al-3.8Cu-1.3Mg-0.5Mn wt. %

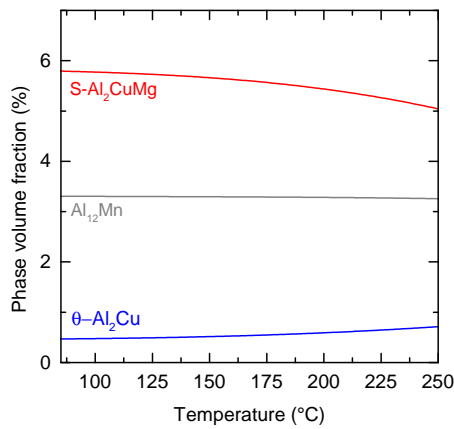


Figure 1: Volume fraction of phases in equilibrium computed for the composition of the matrix in the initial T3 state measured using electron probe microanalyser (Thermo-Calc software with the TCAL4 database).

107 the literature for the same alloy and for similar state (e.g. [14]). According to the literature data,
 108 the first endothermic transformation represents co-clusters dissolution, the second one represents
 109 GPB zones dissolution and the exothermic peak is associated with the formation of the equilibrium
 110 S-Al₂CuMg phase [16]. The endothermic dissolution of S-phase is observed right after S-phase
 111 formation (above 300 °C). One can analyse the obtained experimental curves by fitting the en-
 112 dothermic and exothermic peaks by Gaussian functions (Fig. 2). Such a method allows a clear
 113 distinction between co-clusters and GPB zones dissolution and S-phase formation. One can see
 114 that such a deconvolution of obtained DSC curve by three different Gaussian functions describes
 115 well the heat flux measured as a function of temperature (cumulative curve).

116 DSC curves obtained for AA2024 aged between 85 and 250 °C are shown in Fig. 3. For ease of
 117 reading, the data are presented for the temperature range where the phase transformations of inter-
 118 est were observed: between 160 and 290 °C, according to Fig. 2. Depending on ageing conditions,
 119 one can observe endothermic peaks and/or exothermic peaks or no event. As mentioned earlier,
 120 the first endothermic transformation represents co-clusters dissolution, the second one represents
 121 GPB zones dissolution and the exothermic peak is associated with the formation of the equilibrium
 122 S-Al₂CuMg phase [16]. No results suggesting formation of any other metastable phase (like S')

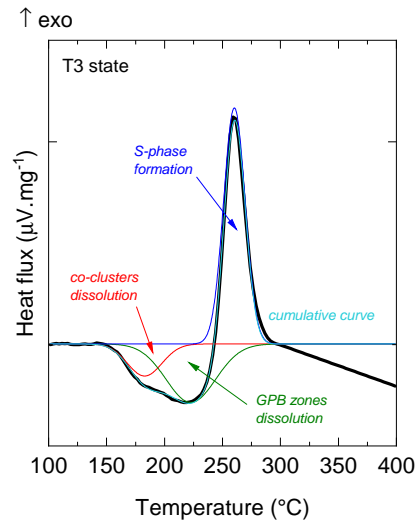


Figure 2: Heat flux as a function of temperature (in black) obtained during DSC experiment with a heating rate of $10\text{ }^{\circ}\text{C min}^{-1}$ for AA2024 at initial T3 state. The heat effect due to co-clusters dissolution (in red), GPB zones dissolution (in green) as well as S-phase formation (in blue) was analysed using Gaussian functions. (For interpretation of the references to colour in this figure legend, the reader is referred to the web version of this article).

123 were obtained in the present study. Moreover, only one peak for S-phase formation was observed
 124 in the present work for all ageing conditions. In some recent studies, two well distinct exothermic
 125 transformations have been observed during heating for model Al-Cu-Mg alloys and were attributed
 126 to the formation of two S-phase types with different orientations, lattice parameters [7, 13–15], or
 127 morphologies (rod and lath like) [12]. Nevertheless, in our case the symmetry of the exothermic
 128 peaks shown in Fig. 3 suggests that only one type of S-phase was formed.

129 Analysing the obtained experimental curves by fitting the endothermic and exothermic peaks
 130 by Gaussian functions (Fig. 3), a clear distinction between co-clusters dissolution (red), GPB zones
 131 dissolution (green) and S-phase formation (blue) can be done. Applying the same analysis to all
 132 the obtained DSC curves, it was possible to conclude about the presence or absence of co-clusters
 133 and GPB zones for different ageing conditions.

134 After ageing at $85\text{ }^{\circ}\text{C}$ for 100, 1000 and 10000 h, the dissolution of both co-clusters and GPB
 135 zones was observed during further DSC analysis. One can see as well that the heat effect due to
 136 co-clusters dissolution decreased, as compared ageing durations of 100 and 10000 h. Therefore,

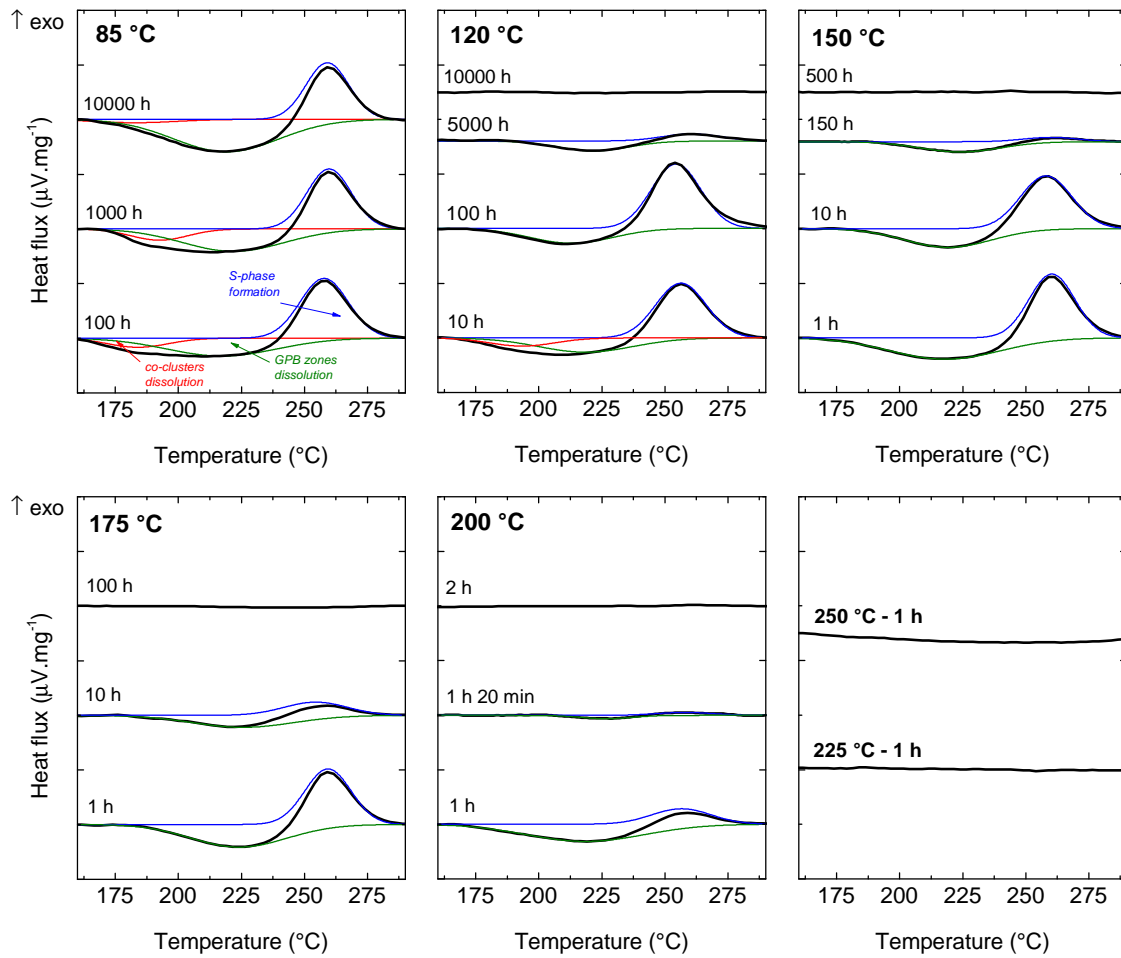


Figure 3: Heat flux as a function of temperature obtained during DSC experiments (black) with a heating rate of $10\text{ }^{\circ}\text{C min}^{-1}$ for AA2024 initially in T3 state after ageing between 85 and 225 $^{\circ}\text{C}$ for different durations. Heat effects corresponding to co-clusters and GPB zones dissolution as well as that corresponding to S-phase formation are deconvoluted using Gaussian function and represented by red, green and blue curves, respectively (the curves are shifted along the y-axis for ease of interpretation). (For interpretation of the references to colour in this figure legend, the reader is referred to the web version of this article).

137 we can conclude, as it was done for initial T3 state (Fig. 2), that co-clusters and GPB zones still
 138 coexist after ageing at 85 $^{\circ}\text{C}$ for durations up to 10000 hours. Ageing of 10 h at 125 $^{\circ}\text{C}$ keeps as
 139 well co-clusters together with GPB zones but the former were not observed from 100 h of ageing
 140 at this temperature indicating that they were completely dissolved during the ageing. Only the
 141 dissolution of metastable GPB zones and formation of stable S-phase were observed after ageing

142 between 100 and 5000 hours at 125 °C with decrease of heat effects with ageing duration increase.
143 Finally, ageing of 10000 h at 125 °C results in almost horizontal DSC curve indicating no effect
144 during DSC experiment and, thus, the alloy had been already in equilibrium state in terms of
145 phases and their fractions. Similar change in DSC curves is observed after ageing at 150, 175
146 and 200 °C: after short ageing durations the dissolution of GPB zones together with formation
147 of S-phase is observed, and for long ageing durations (500 h at 150 °C, 100 h at 175 °C and 2 h
148 at 200 °C), no event is observed on DSC curves. Finally, ageing at high temperatures (225 and
149 250 °C) for 1 h, the shortest duration used, resulted in equilibrium state of AA2024 initially in T3
150 state.

151 Moreover, a careful comparison of the areas under the S-phase formation peaks with respect
152 to ageing duration is presented in Table 1. Depending on ageing conditions these areas can (i)
153 decrease continuously with increase in ageing time (for 150, 175 and 200 °C), (ii) remain stable
154 taking into account experimental uncertainties for a certain ageing duration, then decrease con-
155 tinuously (for 85 and 120 °C) with increase in ageing time and (iii) equal to zero from 1 h of
156 ageing (for 225 and 250 °C). Such a decrease in area under the S-phase formation peaks with
157 ageing duration indicates that some quantity of the S-phase formed during ageing. We conclude
158 that the area under the S-phase peak informs on the quantity of S-phase present in the sample, i.e.
159 the bigger the area observed, the lower the S-phase quantity present after ageing and, thus, before
160 DSC experiment. Remind that a flat DSC curve corresponds to an alloy at equilibrium in terms of
161 nature of phases and their fractions (Fig. 3).

162 One can state a dispersion in the areas under the S-phase formation peak after ageing at 120 °C
163 for the durations up to 1000 h. Further analysis using TEM (see below) permitted to conclude that
164 the S-phase appears from 100 h of ageing at this temperature.

165 The obtained results are summarised in the precipitation map shown in Fig. 4. Five different
166 regions can be identified: S-phase (red squares), S-phase + GPB zones (blue circles), S-phase +
167 GPB zones + co-clusters (orange stars), GPB zones (open diamond) and GPB zones + co-clusters

Table 1: Areas under the peaks corresponding to the formation of the S-phase determined using DSC curves after ageing at different temperatures of AA2024 (0 h corresponds to initial T3 state, measurement uncertainty $\pm 0.1 \mu\text{V } ^\circ\text{C mg}^{-1}$).

Time (h)	Temperature ($^\circ\text{C}$)						
	85	120	150	175	200	225	250
0				2.7			
1	2.7	2.4	2.7	2.6	1.6	0	0
1.3	-	-	-	-	0.2	-	-
6	-	-	-	1.7	-	-	-
10	-	2.5	2.5	0.6	0	-	-
100	2.6	2.9	1.8	0	-	-	-
150	-	-	0.2	-	-	-	-
200	-	-	-	-	-	-	-
500	-	-	0	-	-	-	-
1000	2.4	2.7	0	-	-	-	-
1500	-	1.9	-	-	-	-	-
1990	-	1,8	-	-	-	-	-
5000	2.2	0.4	-	-	-	-	-
10000	2.3	0	-	-	-	-	-

168 (green triangles). The elevated temperatures or long ageing durations result in appearance of
 169 equilibrium S-phase. The formation of the S-phase is preceded by the presence of GPB zones
 170 and co-clusters (as, for example, in the initial T3 state). When temperature and ageing duration
 171 increase, co-clusters disappear leading to the coexistence of the S-phase and GPB zones. It is
 172 worth noting that at 85 $^\circ\text{C}$ the equilibrium S-phase coexists together with metastable co-clusters
 173 and GPB zones from 1000 h of ageing. To the best of the authors knowledge, the formation of
 174 equilibrium S-phase at such a low temperature has never been reported so far. **Indeed, the lowest**
 175 **temperature where the precipitation of S-phase was observed in AA2024 is 170 $^\circ\text{C}$ for the ageing**
 176 **duration of 80 h [8]. The alloy in Ref. [8] was homogenized and quenched without straining**
 177 **indicating an important role of dislocations to induce the precipitation at low temperatures as will**
 178 **be shown further.**

179 The corresponding hardness values are also given in Fig. 4 (above or under the symbol indicat-
 180 ing the region). One can see that the maximum hardness is observed in the S-phase + GPB zones

181 region at the frontier with the S-phase region. Therefore, in AA2024 the maximum mechanical
 182 properties should be associated with the formation of the equilibrium S-phase.

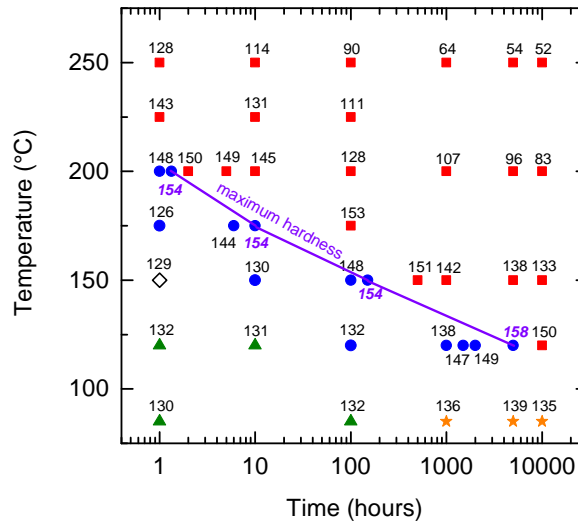


Figure 4: Precipitation map for AA2024 initially in T3 state in the temperature range from 85 to 250 °C for ageing durations from 1 to 10000 hours: red squares: S-phase, blue circles: S-phase + GPB zones, orange stars: S-phase + GPB zones + co-clusters, open diamond: GPB zones, green triangles: GPB zones + co-clusters. The numbers represent the measured hardness values. (For interpretation of the references to colour in this figure legend, the reader is referred to the web version of this article).

183 In order to verify the results obtained by DSC, the microstructure of AA2024 in the different
 184 regions present in Fig. 4 was analysed using TEM. Samples for every region were observed in
 185 high-resolution mode and phase analysis was carried out using Fast Fourier Transformation (FFT)
 186 in the areas of interest (Fig. 5).

187 In the initial T3 state the FFT pattern **constructed for a micrograph obtained with $[001]_{Al}$**
 188 **zone axis** (Fig. 5a) shows the spots corresponding to FCC aluminium solid solution as well as
 189 some additional spots of low intensity. The appearance of such additional spots suggests a local
 190 ordering of the aluminium matrix. Considering that Cu-Cu, Mg-Mg and/or Cu-Mg co-clusters
 191 cannot be easily observed using HRTEM due to their atomic dimensions [19, 20], such an ordering
 192 is attributed to the GPB zones. Moreover, the same spots were found to correspond to GPB

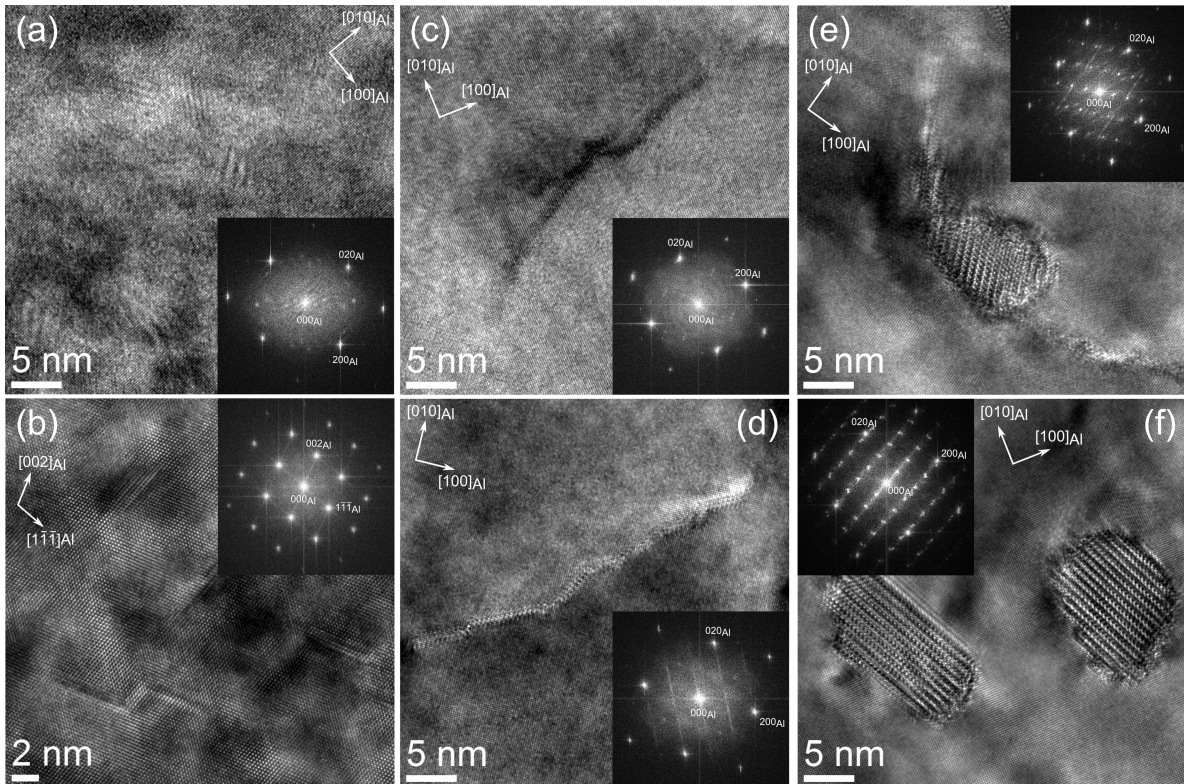


Figure 5: Observations using HRTEM for samples of AA2024 corresponding to different regions in Fig. 4: (a) and (b) initial T3 state (GPB zones + co-clusters), (c) 85 °C for 1000 hours (S-phase + GPB zones + co-clusters), (d) 85 °C for 5000 hours (S-phase + GPB zones + co-clusters), (e) 120 °C for 5000 hours (S-phase + GPB zones) and (f) 200 °C for 100 hours (S-phase). The FFT patterns for the areas of observation are also given for the phase analysis.

193 zones in Ref. [21]. Moreover, a micrograph obtained with $[110]_{Al}$ zone axis (Fig. 5b) revealed
 194 precipitates of thickness of one-two atomic distances which should correspond to GPB zones.

195 After ageing at 85 °C during 1000 and 5000 hours, the formation of the equilibrium S-phase is
 196 observed on dislocations (Fig. 5c and 5d, respectively). A weak series of spots in the FFT pattern in
 197 Fig. 5d correspond to variant 2 of the S-phase, according to Ref. [10]. Therefore, HRTEM analysis
 198 joins the DSC results in confirming that the equilibrium S-phase can be formed at 85 °C. The streak
 199 character of the spots in the FFT patterns is attributed to the very small thickness of the S-phase
 200 precipitates which are at the beginning of their formation. The kinetics of the S-phase formation
 201 at such a low temperature should be governed by pipe diffusion along dislocations. Moreover, an
 202 accurate analysis of the FFT pattern in Fig. 5d shows spots at the $(110)_{Al}$ positions as well. These

203 spots are widely discussed in literature (see, for example, [22, 23]) and are associated to the GPB
204 zones.

205 Ageing at 120 °C during 5000 hours results in appearance of coarse precipitates of S-phase
206 that can be observed near the precipitates previously formed on dislocations (Fig. 5e). The FFT
207 pattern shows well-defined spots corresponding to variant 2 of the S-phase as well as streaks of
208 the S-phase due to the presence of precipitates on dislocations. Moreover, the additional spots at
209 $(110)_{Al}$ positions confirm the presence of GPB zones.

210 Finally, ageing at 200 °C for 100 hours leads to the formation of coarse S-phase (Fig. 5f).
211 The spots in FFT pattern correspond to variant 4 for both of the observed precipitates. No spots
212 corresponding to GPB zones were observed.

213 4. Conclusion

214 In summary, the different regions in the precipitation map for AA2024 initially in T3 state
215 shown in Fig. 4 are confirmed by HRTEM observations. The main results obtained in the present
216 work can be summarized as follows:

- 217 ● at high ageing temperature (from 200 °C and for short and long ageing duration) the equi-
218 librium S-phase precipitates can be observed;
- 219 ● at low ageing temperature (85 and 120 °C) and for short ageing duration (not longer than
220 10 h) co-clusters coexist with GPB zones;
- 221 ● at intermediate ageing conditions (low temperatures/long durations and/or high tempera-
222 tures/short durations) GPB zones coexist with S-phase;
- 223 ● the formation of the equilibrium S-phase was observed, for the first time, at 85 °C as of
224 1000 hours of ageing. It is believed that this is due to dislocation-assisted diffusion.
- 225 ● the maximum hardness for AA2024 for all ageing conditions is located at the frontier be-
226 tween equilibrium S-phase + GPB zones and the S-phase regions.

227 **References**

- 228 [1] E. Starke, J. Staley, *Prog. in Aerospace Sci.* 32 (1996) 131 –72.
- 229 [2] J. C. Williams, E. A. Starke, *Acta Mat.* 51 (2003) 5775 –99. The Golden Jubilee Issue. Selected topics in
230 Materials Science and Engineering: Past, Present and Future.
- 231 [3] N. D. Alexopoulos, Z. Velonaki, C. I. Stergiou, S. K. Kourkoulis, *Mat. Sci. and Eng. A* 700 (2017) 457 –67.
- 232 [4] M. Prudhomme, F. Billy, J. Alexis, G. Benoit, F. Hamon, C. Larignon, G. Odemer, C. Blanc, G. Hénaff, *Int. J.*
233 *of Fat.* 107 (2018) 60 – 71.
- 234 [5] F. Zhang, L. E. Levine, A. J. Allen, C. E. Campbell, A. A. Creuziger, N. Kazantseva, J. Ilavsky, *Acta Mat.* 111
235 (2016) 385 –98.
- 236 [6] I. N. Khan, M. J. Starink, *Mat. Sci. and Tech.* 24 (2008) 1403–10.
- 237 [7] T. Parel, S. Wang, M. Starink, *Materials and Design* 31 (2010) S2 –5. Advanced Component Manufacture from
238 Light Materials.
- 239 [8] G. Sha, R. Marceau, X. Gao, B. Muddle, S. Ringer, *Acta Mat.* 59 (2011) 1659 –70.
- 240 [9] Y. Lin, Y.-C. Xia, Y.-Q. Jiang, H.-M. Zhou, L.-T. Li, *Mat. Sci. and Eng. A* 565 (2013) 420 –9.
- 241 [10] S. C. Wang, M. J. Starink, *Int. Mat. Rev.* 50 (2005) 193–215.
- 242 [11] S. Ringer, K. Hono, *Materials Characterization* 44 (2000) 101–31. doi:[https://doi.org/10.1016/S1044-](https://doi.org/10.1016/S1044-5803(99)00051-0)
243 [5803\(99\)00051-0](https://doi.org/10.1016/S1044-5803(99)00051-0).
- 244 [12] M. Styles, C. Hutchinson, Y. Chen, A. Deschamps, T. Bastow, *Acta Mat.* 60 (2012) 6940 –51.
- 245 [13] M. Styles, R. Marceau, T. Bastow, H. Brand, M. Gibson, C. Hutchinson, *Acta Mat.* 98 (2015) 64 – 80.
- 246 [14] S. Wang, M. Starink, *Acta Mat.* 55 (2007) 933 –41.
- 247 [15] G. Winkelman, K. Raviprasad, B. Muddle, *Acta Mat.* 55 (2007) 3213 –28.
- 248 [16] M. Starink, *Int. Mat. Rev.* 49 (2004) 191–226.
- 249 [17] C. Moy, M. Weiss, J. Xia, G. Sha, S. Ringer, G. Ranzi, *Materials Science and Engineering:*
250 *A* 552 (2012) 48–60. URL: <http://linkinghub.elsevier.com/retrieve/pii/S0921509312006867>.
251 doi:10.1016/j.msea.2012.04.113.
- 252 [18] M. Gao, C. Feng, R. Wei, *Metallurgical and Materials Transactions A* 29 (1998) 1145–51.
- 253 [19] R. Marceau, G. Sha, R. Ferragut, A. Dupasquier, S. Ringer, *Acta Mat.* 58 (2010) 4923 –39.
- 254 [20] R. Marceau, G. Sha, R. Lumley, S. Ringer, *Acta Mat.* 58 (2010) 1795 –805.
- 255 [21] L. Kovarik, S. Court, H. Fraser, M. Mills, *Acta Mat.* 56 (2008) 4804 –15.
- 256 [22] L. Kovarik, P. Gouma, C. Kisielowski, S. Court, M. Mills, *Mat. Sci. and Eng. A* 387-389 (2004) 326 –30.
- 257 [23] S. Wang, M. Starink, *Mat. Sci. and Eng. A* 386 (2004) 156 –63.

Temperature (°C)

